Copper(I) and Copper(II) Complexes of Entwined or Interlocked Phenanthroline Type Ligands: ESR and Crystallographic Investigations

MICHEL GEOFFROY, MICHEL WERMEILLE

Département de Chimie-Physique, 30 Quai Ernest Ansermet, Université de Genève, 1211 Geneva (Switzerland)

CHRISTIANE O. BUCHECKER, JEAN-PIERRE SAUVAGE

Laboratoire de Chimie Organo-Minérale, UA au CNRS 422, Institut de Chimie, 1 rue Blaise Pascal, 67000 Strasbourg (France)

and GÉRALD BERNARDINELLI

Laboratoire de Cristallographie aux Rayons X, 24 Quai Ernest Ansermet, Université de Genève, 1211 Geneva (Switzerland)

(Received May 5, 1989)

Abstract

The crystal structure of $[Cu(dap)_2]BF_4$ has been determined and single crystals of $^{63}Cu(dap)_2BF_4$ were doped with $[^{63}Cu(dap)_2]^{2+}$ ions and studied by ESR. The resulting spectra are compared with those obtained with frozen solutions containing $[^{63}Cu(dap)_2]^{2+}$ or $[Cu(cat\text{-}30)]^{2+}$. The complex $[Cu(dap)_2]^+$ is pseudotetrahedral (crystal structure) as is $[Cu(dap)_2]^{2+}$ in frozen solution. The ^{63}Cu hyperfine coupling shows however that this coordination is not maintained for the dication in a crystalline environment, and the single crystal ESR study suggests the presence of a fifth ligand. Such a versatility of the structure is not observed for the Cu(II) catenate in agreement with the more pronounced rigidity of the interlocked system as compared to its open chain analogue.

Introduction

Although tetracoordinated Cu(II) complexes usually adopt a planar structure, the coordination environment can lead to large tetrahedral distortions. This is particularly the case when bulky substituents are attached to the ligands [1] or when a macrocycle induces strong strain effects [2]. During the last few years these structural distortions have been investigated intensively [1–6] in the context of electron transfer since they can make possible the synthesis of nearly tetrahedral $Cu(I)/Cu(II)N_4$ redox pairs with the same ligand. Moreover specifically strained coordination centres are known to play an important role in biological catalysis [7]. 2,9-Dianisyl-1,10-phenanthroline (dap) (**1**) is potentially a well-suited ligand for the formation of such complexes: previous NMR studies [8] have shown that $[Cu(dap)_2]^+$ is pseudotetrahedral in solution and the successful preparation [9] of the copper(II) catenate $[Cu(cat\text{-}30)]^{2+}$ (**2**) indicates that $[Cu(dap)_2]^{2+}$ is probably not a planar complex. We have therefore tried to study the stereochemistry of this copper(II) complex and have attempted to determine whether the coordination environment can be influenced by an external factor such as the crystal matrix. ESR spectra are very sensitive to structural distortion and are well-suited for the study of copper(II) complexes involving sterically constraining ligands [10]; with this method, however, maximum information is obtained when the paramagnetic species is incorporated as an impurity in a diamagnetic single crystal matrix. In the present study, we have determined the crystal structure of $[Cu(dap)_2]BF_4$ and doped these crystals with the $[Cu(dap)_2]^{2+}$ ion. The resulting ESR tensors are compared with those obtained with frozen solutions containing either the $[Cu(dap)_2]^{2+}$ or the $[Cu(cat\text{-}30)]^{2+}$ complex. They show that the coordination environment of the Cu(II) ion in the dap complex is dependent upon the nature of the host matrix.

Experimental

Compounds

A schematic representation of the dap ligand and of the $[Cu(cat\text{-}30)]^{2+}$ ion is given in Fig. 1. The synthesis of $[Cu(dap)_2]BF_4$ has already been described [8]. $[Cu(dap)_2](ClO_4)_2$ was prepared by mixing two equivalents of dap in solution in CH_2Cl_2 with one equivalent of $Cu(ClO_4)\cdot 6H_2O$ in solution in CH_3OH [9]. $[Cu(cat\text{-}30)]BF_4$ [11] and $[Cu(cat\text{-}30)](ClO_4)_2$ [9] were synthesized following published methods. ^{63}Cu enriched compounds were obtained by using ^{63}CuO (99.7% enrichment, A. Hempel GmbH) as starting material: $[^{63}Cu(dap)_2](BF_4)_2$ was prepared by mixing an aqueous solution of

0020-1693/90/$3.50

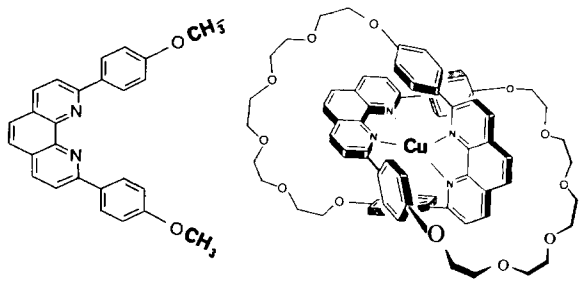

1 2

Fig. 1. Schematic representation of the dap ligand **1** and of the copper catenate **2**.

$^{63}Cu(BF_4)_2 \cdot 6H_2O$ [12]* and dap in solution in CH_2Cl_2. After stirring overnight, the dark green organic layer was decanted, washed once with water and evaporated to dryness. Excess or unreacted dap was eliminated by careful washings of the solid crude complex with hot toluene (yield 28%). $[^{63}Cu(dap)_2](BF_4)$ was obtained by reducing the Cu(II) complex described above with ascorbic acid. The crude dark red copper(I) complex was purified by chromatography (SiO_2, CH_2Cl_2 + 1% MeOH) and recrystallization in CH_2Cl_2–C_6H_6 (yield 40%). Single crystals of $[Cu(dap)_2]BF_4$ were grown by slow evaporation of a solution of this compound in a CH_2Cl_2/benzene mixture. Incorporation of $[Cu(dap)_2]^{2+}$ in single crystals of $[Cu(dap)_2]BF_4$ was performed using a solution containing a mixture of $[Cu(dap)_2](BF_4)_2$ and $[Cu(dap)_2]BF_4$ in the ratio 1/500. A similar process was used to obtain a powder of $[Cu(cat\text{-}30)]BF_4$ doped with $[Cu(cat\text{-}30)]^{2+}$. Crystals of $[Cu(dap)_2](BF_4)_2$ of quality suitable for a crystal structure determination could not be obtained.

Crystal Structure

A dark brown crystal of $[Cu(dap)_2](BF_4)$ was positioned inside a sealed Lindemann capillary tube with traces of the mother liquor. Data were collected at room temperature on a NONIUS CAD4 diffractometer with graphite monochromated Mo Kα radiation (λ = 0.71069 Å). The structure was solved by direct methods (MULTAN-84) [13]. No absorption correction was carried out. Atomic scattering factors and anomalous dispersion terms were taken from the International Tables for X-Ray Crystallography [14]. All coordinates of the H atoms were calculated. The atomic displacement parameters for the non-H atoms were refined as anisotropic for $Cu(dap)_2$ and isotropic for the disordered BF_4 ion. All calculations were performed with the XTAL program [15]. Experimental data and refinement conditions are given in Table 1 and final coordinates are listed in Table 2 according to the atom numbering of Fig. 2.

*Before adding the aqueous $^{63}Cu(BF_4)_2$ solution to the CH_2Cl_2 solution of dap, it is necessary to bring the former acidic solution (pH 1.6) to neutral pH (6.10 to 6.20) by addition of a NaOH solution.

TABLE 1. Summary of crystal data, intensity measurement and structure refinement for $[Cu(dap)_2]BF_4$[a]

Formula	$Cu(C_{52}H_{40}N_4O_4)BF_4$
Molecular weight	935.3
Crystal system	monoclinic
Space group	*I2/a*
Crystal size (mm)	0.25 × 0.50 × 0.70
a (Å)	14.371(4)
b (Å)	16.801(4)
c (Å)	18.001(6)
β (°)	92.23(4)
V (Å^3)	4343(2)
Z	4
D_c (g cm^{-3})	1.43
F(000)	1928
μ (mm^{-1})	0.570
$(\sin\theta/\lambda)_{max}$ (Å^{-1})	0.55
No. measured reflections	3391
No. observed reflections	2424
Criterion for observed	$\lvert F_o\rvert > 4\sigma(F_o)$
No. parameters	301
Refinement (on *F*)	full-matrix
Weighting scheme	$\omega = 1/\sigma^2(F_o)$
H atoms	calculated
Max. and average Δ/σ	0.737, 0.037
Max. and min. $\Delta\rho$ (e Å^{-3})	0.91, −1.28
S	4.07
R, R_w (%)	9.9, 7.0

[a]The cell parameters were determined by least-squares refinement on 24 reflections with 15° < 2θ < 25°.

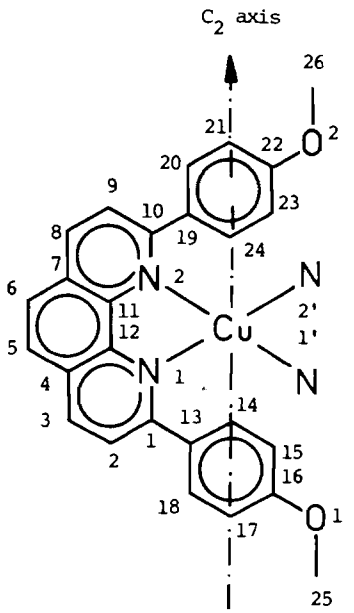

Fig. 2. Numbering of the atoms for the $[Cu(dap)_2]^+$ ion.

TABLE 2. Final coordinates and population parameters for $[Cu(dap)_2]BF_4$ with e.s.d.s in parentheses

Atom	x	y	z	pop
Cu	0.25	0.45487(8)	0.0	
O(1)	0.0479(5)	0.1432(4)	0.1099(4)	
O(2)	0.4056(7)	0.6773(5)	0.2610(5)	
N(1)	0.2257(4)	0.4020(4)	−0.1017(3)	
N(2)	0.3283(4)	0.5314(4)	−0.0622(4)	
C(1)	0.1791(6)	0.3352(5)	−0.1194(5)	
C(2)	0.1620(7)	0.3137(6)	−0.1946(6)	
C(3)	0.1946(9)	0.3592(8)	−0.2491(5)	
C(4)	0.2464(7)	0.4275(6)	−0.2321(5)	
C(5)	0.2837(9)	0.4815(7)	−0.2860(6)	
C(6)	0.3275(9)	0.5486(8)	−0.2666(6)	
C(7)	0.3458(7)	0.5679(6)	−0.1908(6)	
C(8)	0.3898(7)	0.6381(7)	−0.1671(7)	
C(9)	0.4004(6)	0.6541(6)	−0.0942(7)	
C(10)	0.3706(5)	0.5985(5)	−0.0410(5)	
C(11)	0.3140(6)	0.5160(5)	−0.1355(5)	
C(12)	0.2621(6)	0.4467(6)	−0.1564(4)	
C(13)	0.1444(5)	0.2848(5)	−0.0607(5)	
C(14)	0.1117(5)	0.3159(5)	0.0052(5)	
C(15)	0.0829(6)	0.2682(6)	0.0602(5)	
C(16)	0.0806(6)	0.1872(7)	0.0516(7)	
C(17)	0.1110(7)	0.1533(6)	−0.0124(7)	
C(18)	0.1423(6)	0.2026(6)	−0.0679(6)	
C(19)	0.3819(6)	0.6145(5)	0.0375(6)	
C(20)	0.3551(7)	0.6883(6)	0.0655(7)	
C(21)	0.3626(8)	0.7060(6)	0.1375(8)	
C(22)	0.3983(8)	0.6517(7)	0.1876(7)	
C(23)	0.4290(7)	0.5777(6)	0.1634(6)	
C(24)	0.4190(6)	0.5598(5)	0.0883(6)	
C(25)	0.0312(8)	0.0623(8)	0.1003(8)	
C(26)	0.4305(8)	0.6224(7)	0.3124(6)	
B	0.75	0.0878(9)	0.0	
F(1)	0.716(1)	0.1405(8)	0.0485(7)	0.338
F(2)	0.773(1)	0.0208(8)	0.0396(7)	0.327
F(3)	0.787(1)	0.1228(9)	0.0580(8)	0.302
F(4)	0.661(1)	0.114(1)	0.0178(9)	0.283
F(5)	0.694(1)	0.034(1)	0.033(1)	0.237
F(6)	0.829(1)	0.064(1)	0.042(1)	0.257

Electron Spin Resonance

Single crystal ESR spectra were obtained on a VARIAN E-9 spectrometer (X-band, 100 KHz field modulation) equipped with a goniometer which allows the orientation of the crystal in three perpendicular planes without removing the sample from the ESR cavity [16].

The X and Y axes of the ESR reference frame were aligned along the a and b crystallographic reference axes of the $[Cu(dap)_2]BF_4$ crystal respectively. The angular dependence of the ESR spectra was analyzed by using a Hamiltonian which takes into account the electronic Zeeman effect, the nuclear Zeeman effects for copper and the magnetic hyperfine interactions with copper nuclei. The ESR tensors were obtained by using a minimization program which compares the experimental line positions with the line positions calculated by second order perturbation.

Frozen solution (77 K, finger dewar) and powder spectra were recorded on a Bruker 200D spectrometer. Polyoriented spectra were simulated by using a program which adds the contributions of the spectra generated for 120 000 random orientations of the magnetic field. This program enables the calculation with a second order perturbation of the powder spectrum corresponding to the ESR tensors obtained from a single crystal study. When these tensors are not known they were varied to fit the spectrum assuming coincident axial g and copper hyperfine tensors. Such a tensor determination is however somewhat ambiguous since a small rhombic distortion can be masked by a too large linewidth parameter. As previously mentioned [17], only single crystal experiments are well appropriated for the tensors determination of five coordinated Cu(II) complexes adopting a structure intermediate between a square pyramid and a trigonal bipyramid.

Results

Crystal Structure

A stereoscopic view of the $[Cu(dap)_2]^+$ cation is shown in Fig. 3. Selected bond lengths, bond angles and torsional angles are given in Table 3. The copper(I) ion is located on a two-fold axis $(\frac{1}{4}, y, 0)$ and its coordination environment is pseudotetrahedral. The BF_4^- ion is also located on a special position with the boron atom on a C_2 axis $(\frac{3}{4}, y, 0)$. The F atoms are disordered and six distinct positions were observed with refined population parameters varying between 0.237 and 0.338. No solvent or water molecule has cocrystallized with $[Cu(dap)_2]BF_4$.

Electron Spin Resonance

Single crystal ESR study

The linewidths of the ESR signals obtained with a single crystal of $[Cu(dap)_2]BF_4$ doped with the $[Cu(dap)_2]^{2+}$ ion vary with the orientation and are often quite broad. This is due to unresolved hyperfine coupling with the various nitrogen nuclei and to the contribution of the two copper isotopes (^{63}Cu: natural abundance: 69.2%, $I = 3/2$, $g_n = 1.484$, ^{65}Cu: natural abundance: 30.8%, $I = 3/2$, $g_n = 1.588$). In order to improve the precision of the line position measurement we have studied a single crystal of ^{63}Cu enriched $[Cu(dap)_2]BF_4$ doped with $[^{63}Cu(dap)_2]^{2+}$. An example of an ESR spectrum obtained with this system is shown in Fig. 4; for this orientation the two crystallographic sites are magnetically inequivalent and give rise to

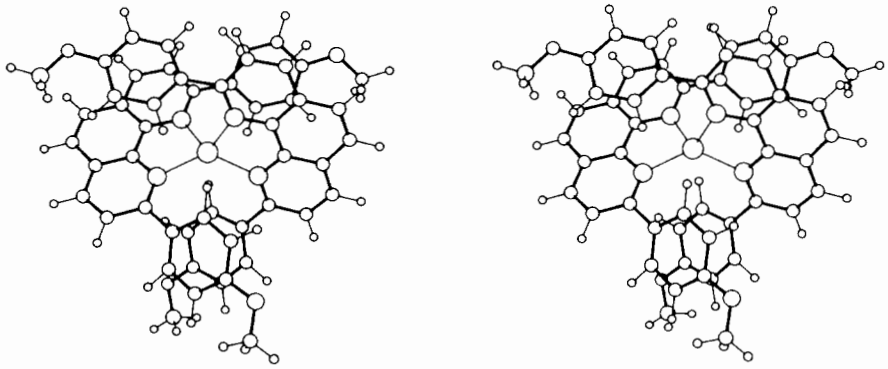

Fig. 3. Stereoscopic view of the $[Cu(dap)_2]^+$ ion.

TABLE 3. Selected bond lengths (Å), bond angles and torsional angles (°) for $[Cu(dap)_2]BF_4$[a]

Cu–N(1)	2.053(6)	N(2)–C(11)	1.353(11)
Cu–N(2)	2.067(6)	O(1)–C(16)	1.381(14)
N(1)–C(1)	1.339(11)	O(1)–C(25)	1.390(15)
N(1)–C(12)	1.359(10)	O(2)–C(22)	1.388(15)
N(2)–C(10)	1.330(11)	O(2)–C(26)	1.345(15)
N(1)–Cu–N(2)	82.1(2)	C(1)–N(1)–C(12)	119.6(7)
N(1)–Cu–N(1′)	128.7(3)	C(10)–N(2)–C(11)	119.6(7)
N(1)–Cu–N(2′)	132.5(2)	C(16)–O(1)–C(25)	119.5(9)
N(2)–Cu–N(2′)	103.0(3)	C(22)–O(2)–C(26)	116.7(9)
C(25)–O(1)–C(16)–C(15)	170.7(9)		
C(26)–O(2)–C(22)–C(23)	−10.6(16)		
N(1)–C(1)–C(13)–C(14)	35.0(12)		
N(2)–C(10)–C(19)–C(20)	−130.0(9)		

[a]Primed atoms are obtained by the symmetry operation: $\frac{1}{2} - x, y, -z$.

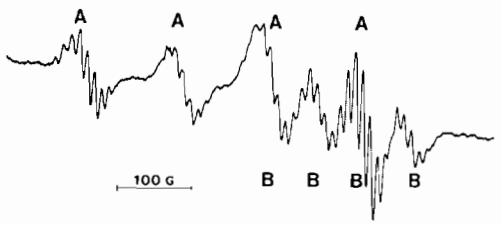

Fig. 4. Example of an ESR spectrum obtained with a single crystal of $[^{63}Cu(dap)_2]BF_4$ doped with $[^{63}Cu(dap)_2]^{2+}$. (A and B are due to two inequivalent orientations of the paramagnetic complex.)

two sets of signals marked A and B, and hyperfine coupling with ^{63}Cu and several ^{14}N nuclei is clearly observed. The angular variation of the ESR signals in the reference planes is shown in Fig. 5. In agreement with the crystal structure (Y aligned along the b axis) the two sites A and B coincide in the XZ plane; this observation is consistent with incorporation of the $[Cu(dap)_2]^{2+}$ dication in the crystal lattice of $[Cu(dap)_2]BF_4$. For some orientations additional lines, of smaller intensity, are also observed; we could not conclude whether they are due to the existence of a small twin or to the presence of another site of incorporation; these additional lines have been detected with several other crystals. The angular dependencies of the A and B lines lead to the g and ^{63}Cu hyperfine tensors shown in Table 4. The ^{14}N hyperfine structure remains unresolved for many orientations and we could not obtain the corresponding hyperfine tensors, nevertheless the maximum ^{14}N splittings are observed for Ho aligned in the bc bissector plane.

Polyoriented samples

All the powder or frozen solution spectra obtained with samples containing $[Cu(dap)_2]^{2+}$ or $[Cu(cat\text{-}30)]^{2+}$ exhibit clearly three discontinuities due to the low field transitions of the 'parallel' hyperfine coupling with copper. The average value of the two corresponding splittings $-(\Delta_{(Gauss)} = (\delta_1 + \delta_2)/2$, Fig. 6) – will be used for the characterization of the various spectra. The ESR spectrum recorded with a powder sample obtained by crushing large single crystals of $[Cu(dap)_2]BF_4$ doped with $[Cu(dap)_2]^{2+}$ and giving rise to signals A and B is shown in Fig. 6(a). This spectrum can be simulated by using the tensors determined in the single crystal ESR study (Fig. 6(b)). The spectrum obtained with

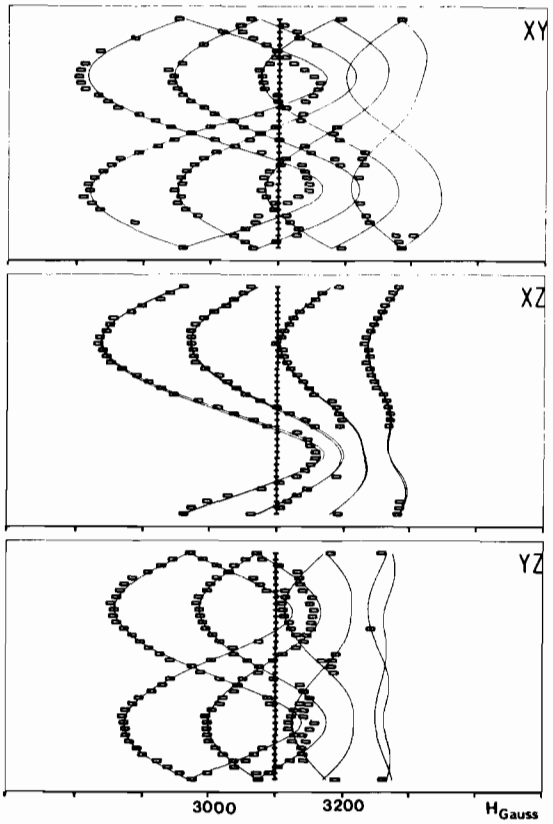

Fig. 5. Angular variations of the signals obtained with a single crystal of $[^{63}Cu(dap)_2]BF_4$ doped with $[^{63}Cu(dap)_2]^{2+}$ (The rectangles correspond to well defined signals which have been used in the optimization process.)

TABLE 4. ESR tensors obtained with a single crystal of $[Cu(dap)_2]BF_4$ doped with $[Cu(dap)_2]^{2+}$ ions

Eigenvalues	Eigenvectors		
g tensor			
$g_1 = 2.0450$	0.7654	±0.6145	0.1907
$g_2 = 2.0768$	−0.2147	±0.5233	−0.8245
$g_3 = 2.2506$	0.6066	∓0.5902	−0.5325
^{63}Cu hyperfine tensor			
$T_1 = 94$ MHz	−0.5514	±0.2060	−0.8083
$T_2 = 138$ MHz	0.5576	±0.8116	−0.1735
$T_3 = 467$ MHz	0.6203	∓0.5465	−0.5625

a frozen solution of $[Cu(dap)_2](BF_4)_2$ in CH_2Cl_2 is shown in Fig. 7(a); it exhibits a Δ splitting equal to 121 G and is practically identical to the spectrum of a frozen solution obtained by dissolving crystals of $[Cu(dap)_2]BF_4$ doped with $[Cu(dap)_2]^{2+}$ (Δ = 123 G). Evaporation of the solvent of the latter solution leads to a Cu(II) spectrum whose three low field discontinuities are clearly observed whereas the high field part ('perpendicular' transitions)

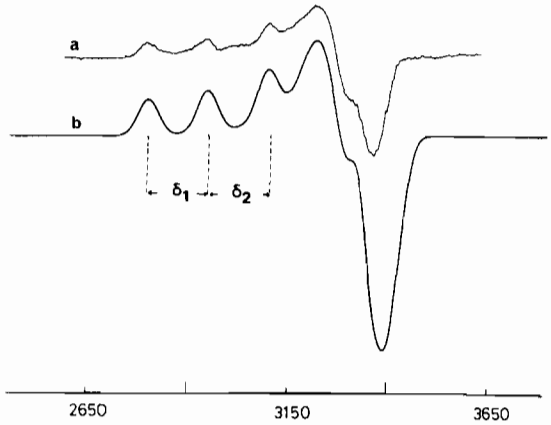

Fig. 6. (a) ESR spectrum recorded with a powder obtained by crushing single crystals of $[^{63}Cu(dap)_2]BF_4$ doped with $[^{63}Cu(dap)_2]^{2+}$. (b) ESR spectrum simulated by using the ESR tensors obtained from the single crystal ESR analysis.

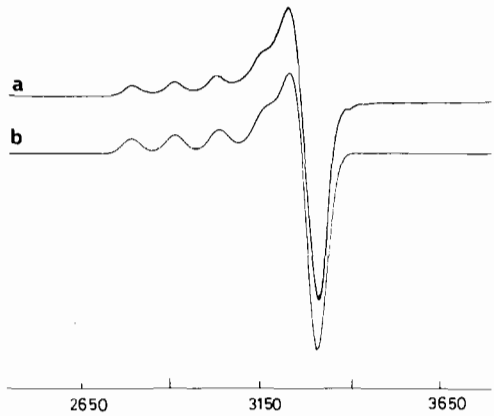

Fig. 7. (a) ESR spectrum obtained with a frozen solution of $[^{63}Cu(dap)_2]^{2+}$. (b) Simulated spectrum obtained with the approximation of coincident axial g and ^{63}Cu-T tensors.

is confused by the presence of additional lines. The relative intensity of these additional signals is not the same for all the samples. Traces of solution remaining at the surface of the grains or a slight transformation of the complex during evaporation could be the cause of this variation. The line positions are not temperature sensitive, but at 77 K the linewidth decreases and some structure due to hyperfine coupling with ^{14}N nuclei is detectable. The Δ parameter (151 G) is close to the splitting observed on the powder obtained by crushing single crystals (Δ = 152 G) but is very different from that measured with the frozen solution (Δ = 123 G). Dissolution of this powder leads to the usual Δ splitting observed with frozen solutions containing $[Cu(dap)_2]^{2+}$ ions. This reversibility is observed for several crystallization–dissolution cycles but care must be taken to avoid humidity; crystallization in the presence of water leads to additional

TABLE 5. ESR tensors obtained with polyoriented samples (approximation of coincident axial tensors)

Sample	$g_\parallel$	$g_\perp$	$T_\parallel$ (MHz)	$T_\perp$ (MHz)
$[Cu(dap)_2]^{2+}$				
Frozen solution[a]	2.277	2.074	390	30
Frozen solution[b]	2.277	2.07	390	32
$[Cu(cat\text{-}30)]^{2+}$				
Frozen solution[a]	2.282	2.076	375	25
Frozen solution[b]	2.281	2.078	370	30
Powder[c]	2.283	2.088	340	45

[a]Solution obtained by dissolving the Cu(II) complex in CH_2Cl_2. [b]Solution obtained by dissolving a powder of the Cu(I) complex doped with the Cu(II) complex (solvent: CH_2Cl_2). [c]Powder of Cu(cat-30)BF_4 doped with $Cu(cat\text{-}30)^{2+}$.

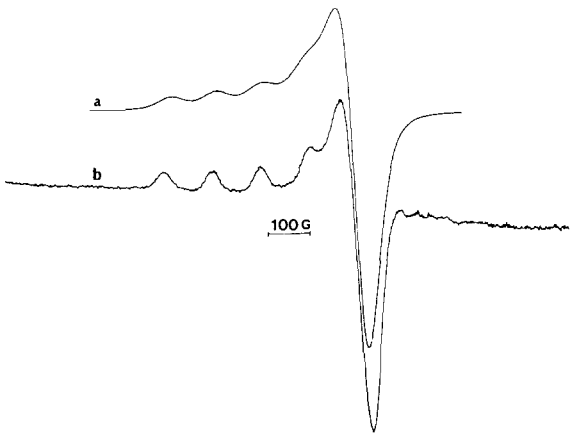

Fig. 8. (a) ESR spectrum obtained with a powder of [Cu(cat-30)]BF_4 crystallized in presence of traces of $[Cu(cat\text{-}30)]^{2+}$. (b) ESR spectrum obtained with a frozen solution of $[Cu(cat\text{-}30)]^{2+}$.

signals in the low field region which are probably due to a transformation product. All the frozen solution spectra have been simulated using the approximation of coincident axial g and Cu hyperfine tensors (e.g. Fig. 7(b)). These tensors are given in Table 5 and, of course, show that the $T_\parallel$ values obtained with polycrystalline samples are appreciably higher than the $T_\parallel$ coupling measured with frozen solutions. Apart from the change in linewidth, the following samples lead to similar ESR spectra: (i) a frozen solution of $[Cu(cat\text{-}30)](ClO_4)_2$ (Fig. 8(b), $\Delta = 117$ G); (ii) a frozen solution of [Cu(cat-30)]BF_4 previously crystallized in the presence of $[Cu(cat\text{-}30)]^{2+}$ ($\Delta = 117$ G); (iii) a powder of [Cu(cat-30)]BF_4 crystallized in the presence of $[Cu(cat\text{-}30)]^{2+}$ ($\Delta = 109$ G, Fig. 8(a)). The corresponding tensors, in the coincident axial tensors approximation, are given in Table 5.

Discussion

The stereochemistry of the metal center in $[Cu(dap)_2]$ can be characterized, for a D_2 symmetry, by the dihedral angle θ between the CuN_2 planes of the two phenanthroline moieties. This angle can vary from 0° (for the planar structure) to 90° (for the totally tetrahedral geometry). For $[Cu(dap)_2]^+$ the crystal structure shows that $\theta = 71.3°$. This stereochemistry is very similar with that found for $[Cu(cat\text{-}30)]^+$ [18] and results, in part, from interactions between the two dap molecules; in particular, the C(13)–C(18) phenyl ring is oriented almost parallel (5.7°) to the C(13′)–C(18′) ring and the distance between the centers of these two rings is only 3.9 Å. This interaction leads to an increase of the tetrahedral angle N(1)CuN(1′) (128.7(3)°) while the opposite angle N(2)CuN(2′) is less constrained (103.0(3)°). It has been recently shown [19] that this intramolecular interaction exists also in catenates as well as the interaction between phenyl C(19)–C(24) and the ring C(7′)–C(11′) of the phenanthroline which is also seen in $[Cu(dap)_2]^+$ (angle between these two rings: 12.7°).

It is well known that for a planar coordination geometry of Cu(II) the ESR tensors exhibit axial symmetry and are characterized by $2.0023 < g_\perp < g_\parallel$ and $Cu\text{-}T_\perp < Cu\text{-}T_\parallel$. Tetrahedral distortion leads to a drastic decrease of $T_\parallel$; for example, in their study of copper(II) tropocoronands complexes Davis *et al.* [2] have shown that a θ increase from 0° to 61° causes a 35% decrease in $T_\parallel$. Knapp *et al.* [4] have recently reported the parameters for the tetrahedral Cu(II) 2,2′-bis(2-imidazolyl)-biphenyl complex; for this system $g_\parallel = 2.32$, $g_\perp = 2.06$, $Cu\text{-}T_\parallel = 353$ MHz whereas the planar tetrakis-(phenylimidazolyl)copper(II) is characterized by $g_\parallel = 2.26$, $g_\perp = 2.08$, $Cu\text{-}T_\parallel = 533$ MHz [20]. The similar values found for frozen solutions of $[Cu(dap)_2]^{2+}$ and $[Cu(cat\text{-}30)]^{2+}$ show that, as for the two corresponding Cu(I) cations, these two complexes have the same stereochemistry. The rather small values of $T_\parallel$ (390 MHz and 370 MHz, Table 5) clearly indicate a pseudotetrahedral coordination for $[Cu(dap)_2]^{2+}$ and $[Cu(cat\text{-}30)]^{2+}$ and show that for these two systems a change in the oxidation state of the metal does not cause a drastic change in the structure of the complex. It may be noticed that the ESR spectra obtained for $[Cu(cat\text{-}30)]^{2+}$ with a frozen solution or a powder have similar $\bar{g}$ and $Cu\text{-}\bar{T}$ tensors ($T_\parallel = 370$ and 340 MHz respectively) and differ only by their linewidth. This means that for this complex the stereochemistry is only weakly affected by the matrix environment.

The ESR spectrum obtained with a powder sample of $[Cu(dap)_2]^+/[Cu(dap)_2]^{2+}$ is appreciably different from that obtained with a frozen solution; there is a large increase of the $T_\parallel$ value which passes

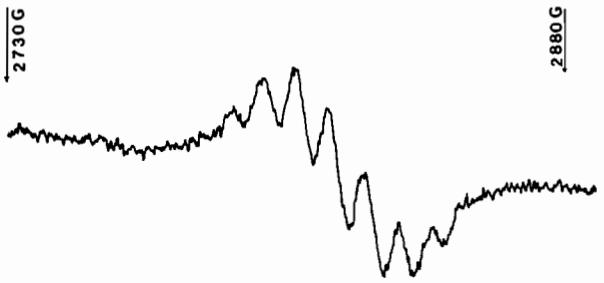

Fig. 9. ^{14}N hyperfine couplings observed on the low field component of the ^{63}Cu hyperfine structure for $[^{63}Cu(dap)_2]^{2+}$ (H_0 is oriented along the ^{63}Cu-T_{max} direction).

from 370 to 467 MHz. The fact that dissolution of the powder leads to the original frozen solution spectrum indicates that the $T_{\parallel}$ variation is not due to a chemical degradation of the $[Cu(dap)_2]^{2+}$ complex but reflects a reversible structure modification occurring during the crystallization. Since the powder ESR spectrum of $[Cu(dap)_2]^{2+}$ can be simulated by using the tensors obtained with a single crystal we will now examine the tensors reported in Table 4. The $\bar{g}$ and Cu-$\bar{T}$ tensors obtained with the single crystal do not display a perfect axial symmetry, nevertheless g_3 and T_3 clearly appear as 'pseudo parallel' eigenvalues and both eigenvectors $\vec{g}_3$ and $\vec{T}_3$ are almost parallel ($\sphericalangle\ g_3, T_3 = 3°$). This T_3 coupling is notably superior to the $T_{\parallel}$ value measured with the frozen solution and can, *a priori*, reflect a considerable flattening of the coordination tetrahedron induced by the crystal packing. Such matrix effects seem however to be less probable since the crystal structure shows that the surrounding $[Cu(dap)_2]^+$ ions have a marked tetrahedral geometry and would rather favor a tetrahedral structure for the guest cation. Moreover, the eigenvector $\vec{T}_3$ is aligned along the crystallographic Cu–N(2′) bond direction and this is not consistent with a simple flattening of the Cu coordination. Another interpretation is that substitution of a monocation $Cu(dap)_2^+$ by a dication $[Cu(dap)_2]^{2+}$ causes a reorganization around the dication and that a fifth ligand is bound (for example an additional BF_4^- assuring the local electric neutrality). In fact, the g and ^{63}Cu coupling tensors measured on the single crystal are very close to the values reported by Bencini *et al.* [17] for copper(II) doped (bis(3-salicyl-aldiminatopropyl methylamine)zinc(II) and are totally consistent with a five coordinate complex intermediate between a square pyramid and a trigonal bipyramid. Surprisingly, when the magnetic field is oriented along the ^{63}Cu-$T_{\parallel}$ direction, the hyperfine coupling with three equivalent ^{14}N is observed (Fig. 9). It could mean that the structure of the trapped complex is close to a square pyramid having a Cu–N bond in axial position. Such a change in the Cu(II) coordination does not occur for the catenate probably as a result of the presence of the two interlocked macrocycles which reduces the accessibility of the copper atom to a fifth ligand and increases the chemical stability of the complex. As expected the geometry of $[Cu(cat\text{-}30)]^{2+}$ is slightly more tetrahedral in the crystalline matrix ($T_{\parallel}$ = 340 MHz), where the neighbour molecules are pseudotetrahedral Cu(I) complexes than in frozen solutions ($T_{\parallel}$ = 370 MHz).

The ESR results reported here show clearly that the complex $[Cu(dap)_2]^{2+}$ in solution adopts a different structure than that found when trapped in a matrix of $[Cu(dap)_2]BF_4$. Surprisingly, however, it is in solution that a pseudotetrahedral structure is found, and in the solid state, surrounded by pseudotetrahedral $[Cu(dap)_2]^+$, that the five coordinate structure is adopted. Burke *et al.* [1] have shown that the cation $[Cu(tmbp)_2]^+$ binds even the weakly coordinating perchlorate anion in the solid state, in agreement with our conclusions. The same authors suggest that a four coordinate structure is therefore improbable in solution, in contradiction with our results which are, moreover, in agreement with studies of Hall *et al.* [21] in nitrobenzene solution. The sensitivity of our solution to humidity during evaporation suggests however that in presence of bases stronger than BF_4^- a five coordinate structure in solution may be adopted. Since a pseudotetrahedral structure has been postulated as a precursor to reduction of Cu(II) [5], it may be anticipated that the pseudotetrahedral solutions of $[Cu(dap)_2]^+$ should show rapid electron transfer kinetics.

Supplementary Material

Tables of complete distances, bond angles, torsional angles, atomic displacements parameters and factor structure can be obtained on request from author G.B.

Acknowledgements

The financial support of the Swiss National Science Foundation is gratefully acknowledged.

References

1 P. J. Burke, K. Henrick and D. R. McMillin, *Inorg. Chem., 21* (1982) 1881.
2 W. M. Davis, A. Zask, K. Nakanishi and S. Lippard, *Inorg. Chem., 24* (1985) 3737.
3 K. D. Karlin, J. C. Hayes, J. P. Hutchinson, J. R. Hyde and J. Zubita, *Inorg. Chim. Acta, 64* (1982) L219.
4 S. Knapp, T. P. Keenan, X. Zhang, R. Fikar, J. A. Potenza and H. J. Schugar, *J. Am. Chem. Soc., 109* (1987) 1882.

5 N. Al-Shatti, A. G. Lappin and A. G. Sykes, *Inorg. Chem., 20* (1981) 1466.
6 R. J. P. Williams, *Inorg. Chim. Acta Rev., 5* (1971) 137.
7 R. J. P. Williams, *J. Mol. Catal., 30* (1985) 1.
8 C. O. Dietrich-Bucheker, P. A. Marnot, J. P. Sauvage, J. P. Kintzinger and P. Maltesse, *Nouv. J. Chim., 8* (1984) 573.
9 C. O. Dietrich-Bucheker, J. P. Sauvage and J. M. Kern, *J. Am. Chem. Soc., 111* (1989) 7791.
10 A. Bencini and D. Gatteschi, *Transition Met. Chem., 8* (1982) 127.
11 C. O. Dietrich-Bucheker, J. P. Sauvage and J. P. Kintzinger, *Tetrahedron Lett., 24* (1983) 5095.
12 H. Funk and F. Binder, *Z. Anorg. Allg. Chem., 159* (1927) 121.
13 P. Main, S. J. Fiske, S. E. Hull, L. Lessinger, G. Germain, J. P. Declercq and M. M. Woolfson, *A System of Computer Programs for the Automatic Solution of Crystal Structures from X-Ray Diffraction Data,* Universities of York, U.K., and Louvain-la-Neuve, Belgium, 1980.
14 *International Tables for X-Ray Crystallography,* Vol. IV, Kynoch Press, Birmingham, 1974.
15 S. R. Hall and J. M. Stewart (eds.), *XTAL2.2 User's Manual,* Universities of Western Australia, and Maryland, U.S.A., 1987.
16 T. Berclaz, J. Diolot, M. Geoffroy and L. Ginet, *J. Phys. E, 10* (1977) 871.
17 A. Bencini, I. Bertini, D. Gatteschi and A. Scozzafava, *Inorg. Chem., 17* (1978) 3194.
18 M. Cesario, C. O. Dietrich-Buchecker, T. Guilhem, C. Pascard and J. P. Sauvage, *J. Chem. Soc. Chem. Commun.,* (1985) 244.
19 M. Cesario, C. O. Dietrich, A. Edel, J. Guilhem, J. P. Kintzinger, C. Pascard and J. P. Sauvage, *J. Am. Chem. Soc., 108* (1986) 6250.
20 H. J. Prochoska, W. F. Schwindinger, M. Schwartz, M. J. Brok, E. Bernarducci, R. A. Lalancette, J. A. Potenza and H. J. J. Schugar, *J. Am. Chem. Soc., 103* (1981) 3446.
21 J. R. Hall, M. R. Litzow and R. A. Plowman, *Aust. J. Chem., 18* (1965) 1331.